

1    **Timing and Climatic-driven Mechanisms of Glacier Advances in Bhutanese Himalaya during the Little Ice Age**

2    Weilin Yang<sup>1</sup>, Yingkui Li<sup>2</sup>, Gengnian Liu<sup>1</sup>, Wenchao Chu<sup>3</sup>

3    <sup>1</sup>College of Urban and Environmental Sciences, Peking University, Beijing 100871, China.

4    <sup>2</sup>Department of Geography, University of Tennessee, Knoxville, TN 37996, USA.

5    <sup>3</sup>Department of Earth System Science, Ministry of Education Key Laboratory for Earth System Modeling, Institute for Global  
6    Change Studies, Tsinghua University, Beijing 100084, China.

7    *Correspondence to:* Wenchao Chu (peterchuwenchao@foxmail.com)

8    **Abstract.** Mountain glaciers provide us a window into past climate changes and landscape **evolution**, but the pattern of glacier  
9    evolution at centennial or suborbital timescale remains elusive, especially in monsoonal Himalayas. We simulated the glacier  
10   evolution in Bhutanese Himalaya (**BH**), a typical monsoon influenced region, during the Little Ice Age (LIA) using the Open  
11   Global Glacier Model driven by six paleo-climate datasets and their average. Compared with geomorphologically-mapped  
12   glacial landforms, the model can well capture the patterns of glacier length change. Simulation results revealed four glacial  
13   substages (1270s, 1470s, 1710s, and 1850s) during LIA in the study area. Statistically, a positive correlation between the  
14   number of glacial substages and glacier slope was found, indicating the occurrence of glacial substages might be a result from  
15   heterogeneous responses of glaciers to climate change. **Monthly climate change analysis and sensitivity experiments indicated**  
16   summer temperature **largely** dominates the regional glacier evolution during the LIA **in BH**.

17    **1 Introduction**

18    Mountain glaciers over high Himalayas provide us a critical window to explore the linkage between climatic, tectonic,  
19   and glacial systems (Oerlemans et al., 1998; Owen et al., 2009; Dortch et al., 2013; Owen & Dortch, 2014; Saha et al., 2018).  
20   Many scientists have investigated the glacial history **of the Himalaya** at orbital-scale, indicating that a general trend of glacier  
21   advances is related to overall summer temperature, forced by orbitally-controlled insolation (Murari et al., 2014; Yan et al.,  
22   2018, 2020, 2021). However, latest observations with finer temporal resolution have revealed that the evolution of some  
23   glaciers in monsoonal Himalayas has suborbital-scale fluctuations, which **has generated increasing interest in exploring its**  
24   **mechanisms** (Solomina et al., 2015; Peng et al., 2020).

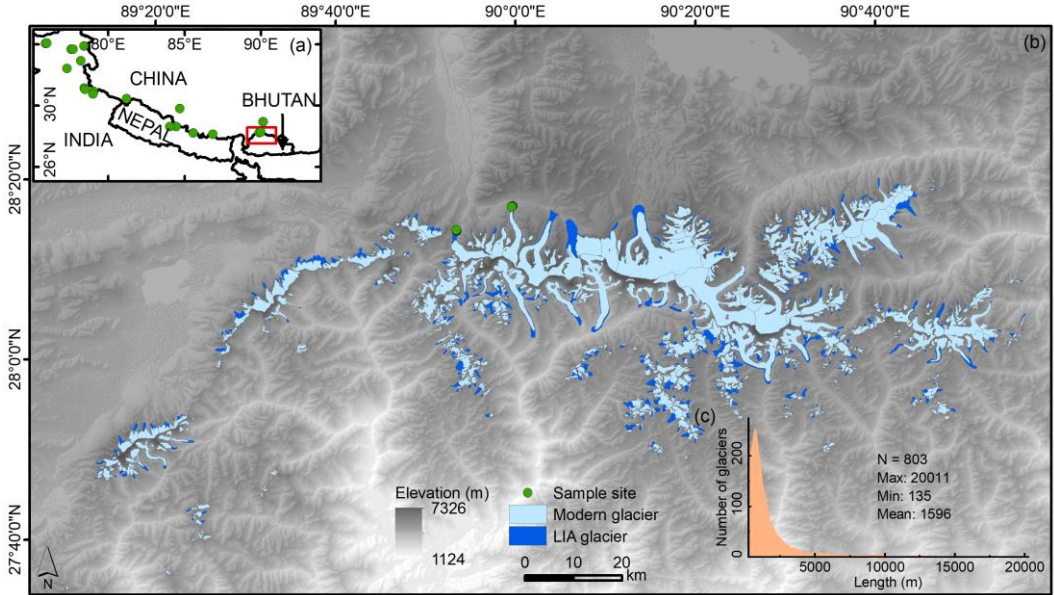
25    The Little Ice Age (LIA; from 1300 to 1850 CE; Grove, 2013; Qureshi et al., 2021) is the latest cooling event during the  
26   Holocene, during which most mountain glaciers advanced, forming abundant well-preserved and distinctive geomorphic  
27   landforms (Murari et al., 2014; Qiao & Yi, 2017; Peng et al., 2019, 2020). Previous studies have reconstructed the timing and  
28   extent of glacier evolution during the LIA based on field investigation, geomorphological mapping, and cosmogenic nuclide  
29   dating (Owen & Dortch, 2014 and references therein; Zhang et al., 2018a, 2018b; Carrivick et al., 2019; Qureshi et al., 2021).  
30   However, it is still unclear how many substages (glacial advances) exist during the LIA (Yi et al., 2008; Murari et al., 2014;

31 Xu & Yi, 2014), due to the **post-glacial** degradation and the large uncertainties in the dating methods (Heyman et al., 2011; Fu  
32 et al., 2013). In addition, Carrivick et al. (2019) indicated that the reconstructions using individual glaciers or a small number  
33 of glaciers may be not representative for the regional average.

34 Numerical glacial modelling is a powerful way to study glacier evolution on centennial timescale (Parkes & Goosse, 2020)  
35 and quantify the response of glaciers to climate change (Eis et al., 2019). **It can also be a complement for field-based approach**  
36 **in capturing the glacier evolution on regional scale.** Meanwhile, the model simulations can be evaluated via multiple  
37 observations to ensure the reliability. However, evaluating the simulation results is still challenging due to the scarcity of the  
38 direct observational record for glacier changes during the LIA (Goosse et al., 2018).

39 Based on the above issues, this study **provides** a possible approach on how to bring observation and simulation together,  
40 what the contribution of individual glacier to regional glacier evolution is, and how climate change drives glacier evolution  
41 (Goosse et al., 2018; Carrivick et al., 2019; Peng et al., 2019, 2020). We chose a typical monsoon-influenced area, Bhutanese  
42 Himalaya (BH) as an example, using the Open Global Glacier Model (OGGM) to improve our **understanding** on the pattern  
43 of LIA glacier changes (Fig. 1). The BH (27.5~28.3°N, 89.1~91.0°E) is an east-west-trending mountain range with an average  
44 elevation above 5000 m above sea level (a.s.l.), nourishing abundant high mountain glaciers (Peng et al., 2019, 2020; Fig. 1b).  
45 According to the Randolph Glacier Inventory V6.2 (RGI; RGI Consortium, 2017), there **are** 803 modern glaciers in BH,  
46 covering an area of  $\sim 1233.685 \text{ km}^2$  (Fig. 1b). Fifty-seven glaciers belong to RGI13 region (Central Asia) and 746 glaciers  
47 belong to RGI15 region (South Asia East). The distribution of glacier length is shown in Fig. 1c with an average length of  
48 1596 m (950 m for the median value) ranging from 135 m to 20011 m. **Small** glaciers (length shorter than 3000 m) are prevalent  
49 in BH (accounting for 88.9 %).

50 We systematically simulated the BH glacier changes during the LIA based on the climate data from six different general  
51 circulation models (GCMs) and their average. The simulated glacier length changes are validated by geomorphological maps  
52 and previous studies. The pattern of regional glacial evolution is compared with  $^{10}\text{Be}$  and  $^{14}\text{C}$  glacial chronologies across the  
53 monsoon influenced Himalayas. The dominant climatic factors of BH glacial evolution are explored through analyzing the  
54 glacier surface mass balance (SMB) changes and a series of sensitivity experiments.



55

56 Figure 1. An overview of study area and moraine sites. The red box in (a) shows the location of the study area and the green  
 57 circles in (a) displays the spatial distribution of the  $^{10}\text{Be}$  exposure dating moraines. The basic information of these moraine  
 58 sites can refer to Table S1. (b) The extent of the modern glaciers (in light blue; RGI Consortium, 2017) and LIA glacier (in  
 59 navy blue). The background DEM is obtained from the Shuttle Radar Topography Mission (SRTM) 90 m Digital Elevation  
 60 Model v4.1 (Jarvis et al., 2008; <http://srtm.csi.cgiar.org/>). (c) The length distribution of modern glaciers.

## 61 2 Methods

### 62 2.2 Model Description

63 The OGGM (v1.50) is a 1.5D ice-flow model, able to simulate past and future mass-balance, volume, and geometry of  
 64 glaciers (Maussion et al., 2019). Previous studies have confirmed a good performance of this model in simulating alpine  
 65 glaciers (Farinotti et al., 2017; Pelto et al., 2020) and reproducing the millennial trend of glacial evolution in mountainous  
 66 regions (Goosse et al., 2018; Parkes & Goosse, 2020). For example, OGGM has been successfully applied to simulate High  
 67 Mountain Asia glaciers, including their thickness, velocity, and future evolutions (Dixit et al., 2021; Pronk et al., 2021;  
 68 Shafeeqe & Luo, 2021; Furian et al., 2022; Chen et al., 2022).

69 The OGGM couples a surface mass balance (SMB) scheme with a dynamic core (Marzeion et al., 2012; Maussion et al.,  
 70 2019). The dynamic core adopts the shallow-ice approximation (SIA), computing the depth-integrated ice flux of each cross-  
 71 section along multiple connected flowlines diagnosed by a pre-process algorithm (via geometrical centerlines). Two key  
 72 parameters, the creep parameter  $A$  and the sliding parameter  $f_s$ , in the dynamic core are set to their default values ( $A = 2.4 \times$   
 73  $10^{-24} \text{ s}^{-1} \text{ Pa}^{-3}$ ,  $f_s = 0 \text{ s}^{-1} \text{ Pa}^{-3}$ , without lateral drag). The spatial resolution ( $dx$ ; m) of the target grid is scale dependent, determined  
 74 by the size of the glacier ( $dx = 14\sqrt{S}$ , with  $S$  representing the glacier area in  $\text{km}^2$ ) but truncated by minimum (10 m) and  
 75 maximum (200 m) values, respectively (Maussion et al., 2019). According to the observations, the largest simulation domain  
 76 is set to 160 grid points outside the modern glacier boundaries to ensure that the domain is large enough for the LIA glaciers.  
 77 If a glacier advance **exceeds** the domain during the simulation, we will exclude this glacier in the further analysis due to its

78 large simulation bias.

79 The ice accumulation is estimated by a solid precipitation scheme to separate the total precipitation into rain and snow  
80 based on monthly air temperature. In this scheme, the amount of solid precipitation is computed as a fraction of the total  
81 precipitation. Specifically, precipitation is entirely solid if  $T_i \leq T_{Solid}$  (default setting is 0 °C), entirely liquid if  $T_i \geq T_{Liquid}$   
82 (defaults to 2 °C) or divided into solid and liquid parts based on a linear relationship with those two temperature values. The  
83 ablation is estimated using a positive degree-day (PDD) scheme (Eq. 1). Melting occurs if monthly temperature ( $T_i(z)$ ) is above  
84  $T_{melt}$ , which is equal to -1 °C.

85 
$$m_i(z) = p_f P_i^{solid}(z) - \mu^* \cdot \max(T_i(z) + \beta, 0) + \varepsilon, \quad (1)$$

86 where  $m_i(z)$  is the monthly SMB at elevation  $z$  of month  $i$ .  $P_i^{solid}(z)$  is the monthly solid precipitation, and  $p_f$  is a general  
87 precipitation correction factor (default setting is 2.5).  $\mu^*$  is the temperature sensitivity parameter and  $\beta$  is the temperature bias.  
88 A residual bias term ( $\varepsilon$ ) is added as a tuning parameter to represent the collective effects of non-climate factors (Marzeion et  
89 al., 2012; Maussion et al., 2019). Different from the conventional PDD schemes embedded in other ice sheet models, such as  
90 Parallel Ice Sheet Model (Bueler & Brown, 2009; Winkelmann et al., 2011), SICOPOLIS (Greve, 1997a, 1997b) or CISM  
91 (Lipscomb et al., 2019), that assume  $\varepsilon$  and  $\mu^*$  as constant values, these parameters vary with glacier in OGGM.

92 The monthly temperature and precipitation from six different GCMs (BCC, CCSM4, CESM, GISS, IPSL, and MPI),  
93 covering a period from 850 CE to 2000 CE, are used to drive OGGM. These data are available in the Past Model  
94 Intercomparison Project (PMIP3) and the Coupled Model Intercomparison Project (CMIP5) protocols (Schmidt et al., 2012;  
95 Tayloret al., 2012; PAGES 2k-PMIP3 group, 2015) – with details listed in Goosse et al. (2018) and Table S2. The climate data  
96 cannot be directly used in glacial model due to the large systematical bias of GCMs. A calibration algorithm is adopted by  
97 OGGM to correct the GCMs climate data by taking the anomalies between GCMs and the Climate Research Unit (CRU) TS  
98 4.01 (Harris et al., 2020) mean climate from 1961 to 1990 (Parkes & Goosse, 2020). In addition, the mean climate (MC) from  
99 six different GCMs is also calculated and calibrated to drive OGGM (hereafter MC experiment) to further alleviate the climate  
100 bias of each GCM. Therefore, we would focus on analyzing the results from MC experiment, but also involve some discussions  
101 on the difference between MC experiment and six GCM experiments.

## 102 **2.2 Identification of the Glacial Substages and Related Concepts**

103 Similar to Goosse et al. (2018) and Parkes & Goosse (2020), we use simulated glacier length change ( $\Delta L = L - L_{1950}$ ),  
104 where  $L_{1950}$  represents the simulated glacier length at 1950 to represent glacier evolution. In order to alleviate the influence  
105 of glacier size (length) to the mean value, we further convert  $\Delta L$  into *glacier length change ratio* ( $GLR = \frac{\Delta L}{L_{1950}}$ ). Firstly, we  
106 exclude the glaciers of which the simulated lengths equal to zero at 1950 because these glaciers have large simulation biases  
107 according to the observations (RGI). Then, decadal mean GLR is calculated for each glacier in order to remove the interannual

108 variabilities. Next, the Gaussian Filter (with standard deviation setting to be 3) is applied to the decadal mean GLR for each  
109 glacier to extract the main oscillations. After that, we obtain the regional average GLR by averaging all glaciers' GLR (decadal  
110 averaged and Gaussian Filtered) within the domain. Finally, we try to find all peaks and their corresponding times in the  
111 regional average GLR timeseries based on the “findpeaks” function embedded in Matlab Software. **A local peak is a data**  
112 **sample that is larger than its two neighboring samples. We set the minimum peak prominence to 0.2 to eliminate the peaks that**  
113 **drop smaller than 0.2 on either side.** Each peak found is defined as a *glacial substage* during the LIA. We name the substages  
114 from new to old (LIA-1, LIA-2, LIA-3, LIA-4 and maybe more).

115 A concept related to GLR is *maximum peak GLR*, defined as the GLR when a glacier reaches its maximum peak during  
116 a period. Notice that *maximum peak GLR* is different from the maximum GLR. For example, in Fig. 2d, the *maximum peak*  
117 *GLR* occurs around 1270 CE rather than 1100 CE. Based on this concept, the simulated *second/third/fourth peak GLR* is  
118 defined as the GLR when a glacier reaches its second/third/fourth maximum peak during a period.

### 119 2.3 Spinup, Tuning Strategy, and Experiment Design

120 We spinup the model to avoid the influence of the **pre-run** condition and tuned the parameter, temperature bias ( $\beta$ ) in Eq.  
121 1, to obtain a better **post-spinup** condition. Note that **post-spinup condition would be used as the initial condition for the**  
122 **historical run.** The  $\beta$  directly regulates **the post-spinup condition** and largely impacts the *GLR* during early LIA (e.g., LIA4).  
123 We alter  $\beta$  from -1 to 1 °C with an increment of 0.1 °C during the spinup period to select the best initial condition for the  
124 historical run. For all experiments, a 5000-year spin-up forced by the climate data selected randomly from a 51-year window  
125 of 875 - 925 CE is conducted prior to the historical run. After spinup, we model the LIA glacier changes with  $\beta = 0$ , forced by  
126 the past climate time series from 900 to 2000 CE. In addition, we start our analysis at the year 1100 for a better display of the  
127 glacial fluctuations during the LIA (1300-1850 CE; Grove, 2013; Qureshi et al., 2021).

128 The tuning procedure is based on MC experiment while six GCM experiments share the same  $\beta$  with MC experiment  
129 during spinup period. Our tuning strategy is threefold. First, we should ensure the regional average *GLR* is larger during LIA4  
130 than LIA1 as in the observations because previous studies indicated that the majority of glaciers advanced to their LIA  
131 maximum extents at the early LIA rather than the late LIA (Murari et al., 2014; Xu & Yi, 2014). Second, we need to ensure  
132 the simulated *maximum peak GLR* closer to the observations. Notice that we choose to use *maximum peak GLR* because the  
133 observations derived from the geomorphological mapping methods can only obtain this variable during LIA (Section 2.4).  
134 Third, let more glaciers be available in the analysis as a smaller  $\beta$  will decrease the number of available glaciers (Fig. 2c).

135 A series of sensitivity experiments are also conducted to further validate the effect of climate changes on BH glacier  
136 advances on both seasonal and annual scales. We apply a ‘constant climate scenario’, using the CRU datasets as the climate  
137 forcing, and run the simulation until reaching equilibrium (here 5000 years). The window size **of CRU data** is set to 51-year  
138 and centered on  $t^*$ .  $t^*$  is year when the model best reproduces the observed SMB for glaciers in the World Glacier

139 Monitoring Service (WGMS; WGMS, 2017) datasets (Marzeion et al., 2012; Maussion et al., 2019). We set  $\varepsilon$  to 0 in Eq. 1  
140 in order to maintain the contemporary glacier geometry under the contemporary climate condition. The control experiment is  
141 forced by the default monthly temperature and precipitation. Keeping the same precipitation, we alter  $\beta$  from -1 to 1 °C with  
142 an increment of 0.1 °C to the original seasonal/annual temperature to test the sensitivity of temperature on glacier evolution.  
143 The similar approach is also applied to the precipitation. Holding the temperature, we adjust the precipitation from -20 to 20 %  
144 with an increment of 2 % in the original seasonal/annual precipitation data.

145 **2.4 Establishing Regional Chronology and Mapping LIA Glacier**

146 The simulated timing and extent of glacial advances are validated with the  $^{10}\text{Be}$  surface exposure ages and  $^{14}\text{C}$  ages of  
147 the LIA moraines across the monsoonal Himalaya and the mapped LIA glaciers over BH. Here, we assume that the dated  
148 moraines outside of the study area also can represent the dates of glacial advances within the study area because the terrain  
149 and climatic conditions are similar (Owen & Dortch 2014; Murari et al., 2014). With this assumption, more observations can  
150 be included in this study, making them more representative of regional features. Five  $^{10}\text{Be}$  ages from moraine M1 of Cogarbu  
151 valley and seven  $^{10}\text{Be}$  ages from moraine M1 of Shi Mo valley were selected to determine the regional glaciation chronology  
152 establishing in BH (Fig. 1b and Fig. S1), and 126  $^{10}\text{Be}$  surface exposure ages and 7  $^{14}\text{C}$  across the monsoonal Himalayas are  
153 used as a supplement (Fig. 1a; Table S1; Xu & Yi, 2014).

154 All  $^{10}\text{Be}$  ages are recalculated using CRONUS Earth V3 online calculator with the time and nuclide-dependent scaling  
155 scheme ‘LSDn’ (Balco et al., 2008; Lifton, et al., 2014; <http://hess.ess.washington.edu/math/>). We then adopt the method  
156 advocated by Chevalier et al. (2011) and Dong et al. (2018) to exclude the potential outliers. The potential outliers are defined  
157 as the  $^{10}\text{Be}$  ages which did not overlap within 1  $\sigma$  external uncertainty with others for a moraine. After removing outliers, we  
158 use the oldest age of a moraine sample set to represent the moraine depositional age (Chevalier et al., 2011; Dong et al., 2018;  
159 Peng et al., 2020).

160 Based on regional glacial chronology and the evidence of sediment-landform assemblages (Chandler et al., 2019), we  
161 map the outermost lateral and terminal moraines in BH to represent the maximum extent of glaciers during the LIA (the  
162 *maximum peak GLR*). These moraines are usually well-preserved with sharp crests, locating from several hundred meters to a  
163 few kilometers away from the termini of modern glaciers, and damming a lake in front of modern glaciers (Qiao & Yi, 2017;  
164 Zhang et al., 2018b; Qureshi et al., 2021). We use the world imagery ESRI ([http://goto.arcgisonline.com/maps/World\\_Imagery](http://goto.arcgisonline.com/maps/World_Imagery))  
165 and Google Earth high-resolution imagery to delineate the LIA moraines and outlines. However, not all LIA glaciers could be  
166 identified due to the destruction of moraines. Only 408 glaciers of the 803 BH glaciers could be mapped (Fig. 1b). The length  
167 of contemporary glaciers is provided in Randolph Glacier Inventory V6.2 datasets (RGI; RGI Consortium, 2017), and that of  
168 the LIA glaciers is calculated in ArcGIS based on the main model flowline in OGGM.

169 **3 Results**170 **3.1 The Choice of Post-Spinup Condition**

171 In order to obtain a better estimation of the **post-spinup** condition, we tuned the  $\beta$  during the spinup period. As shown in  
 172 Fig. 2,  $\beta$  strongly influences the **post-spinup** condition and thus the LIA simulation results, especially for the first 600 years  
 173 (Fig. 2b). With a decreased  $\beta$ , the regional average glacier volume increases (Fig. 2a), but the number of available glaciers (i.e.,  
 174 glaciers which do not exceed the prescribed domain boundaries) decreases during the spinup period (Fig. 2c). The number of  
 175 available glaciers for the LIA simulation is approximately equal to that during the spinup period, except for a reduction when  
 176  $\beta$  is positive (Fig. 2c). This is probably because smaller  $\beta$  can kick out the glaciers which would potentially suffer from large  
 177 simulation bias during LIA simulation. In addition, more glaciers disappear in 1950 ( $Length_{1950} = 0$ ; Fig. 2c) with a larger  $\beta$ .  
 178 Note that the model is unable to capture some small glaciers, which rely on local topography, preferential deposition and  
 179 redistribution of snow, or avalanching for their existence.

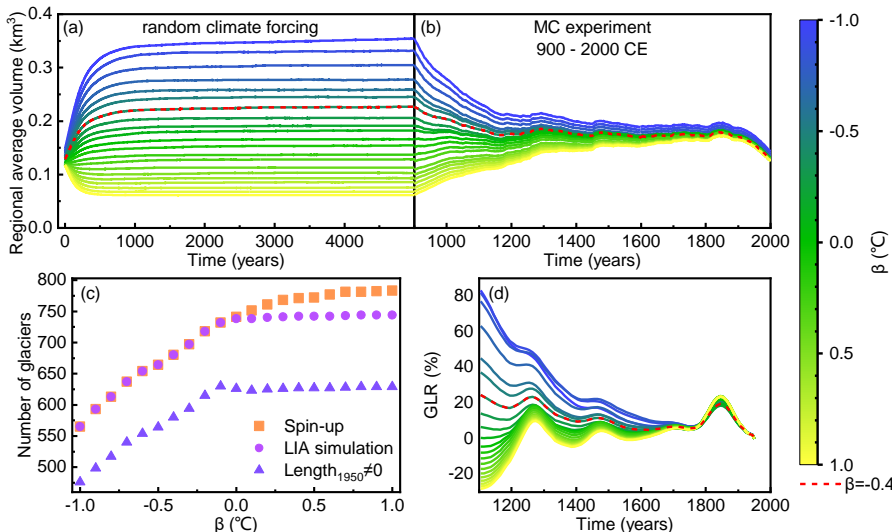
180 **Post-spinup** condition slightly impacts the time and number of glacial substages but largely influences the strength of  
 181 glacial substages (GLR) during LIA simulation (Fig. 2d; Fig. S1). Four substages occurred at  $\sim$ 1250s – 1280s (LIA-4),  $\sim$ 1470s  
 182 – 1480s (LIA-3),  $\sim$ 1700s – 1720s (LIA-2) and  $\sim$ 1850s (LIA-1) are detected under a wide range of  $\beta$  (from  $-0.7$   $^{\circ}$ C to  $1.0$   $^{\circ}$ C)  
 183 in the MC experiment. However, the number of substages become less when  $\beta$  is smaller than  $-0.7$ . Only two substages have  
 184 been detected with  $\beta = -0.8$  (LIA2 and LIA1) and  $\beta = -1.0$  (LIA3 and LIA1) while only the latest substage could be probed  
 185 with  $\beta = -0.9$ . This is because smaller  $\beta$  would cause excessively large initial glaciers so that a smaller climate perturbation is  
 186 not powerful enough for the glaciers to stop retreating during the early LIA period. In addition, the occurrence time of LIA-  
 187 4, LIA-3, and LIA-2 becomes earlier with a smaller  $\beta$ , but the occurrence time of LIA-1 is stable with various  $\beta$ .

188 The GLR during the early LIA periods (LIA-4 and LIA-3) are strongly regulated by the **post-spinup** condition (Fig. 2d).  
 189 Smaller  $\beta$  will lead to a larger GLR during LIA-4 and LIA-3. According to the tuning strategies in Section 2.3, simulations  
 190 with  $\beta \geq -0.3$  should be excluded as larger GLR must be ensured during LIA-4 than LIA-1. The Root Mean Squared Error  
 191 (RMSE) of *maximum peak GLR* between the simulation and observation is smallest when  $\beta = -0.4$  (RMSE = 133.1 %), though  
 192 a decreasing trend is found when  $\beta \leq -0.8$  (Fig. 3). However, the number of available glaciers when  $\beta \leq -0.8$  is less than that  
 193 when  $\beta = -0.4$ . Therefore, we finally choose the simulation results with  $\beta = -0.4$  based on the tuning strategies.

194 The modern ice volume is estimated by the ice inversion module in OGGM (Maussion et al., 2019). This module is  
 195 designed to diagnose the glacier thickness distribution under the constraints of modern glacier extents (such as RGI outlines)  
 196 and climate scenario (such as CRU dataset), which can provide the best estimation of glacier volume (Maussion et al., 2019;  
 197 Farinotti et al., 2019). The simulated BH ice volume at 2000 increases with decreased  $\beta$ , results from the reduction of available  
 198 glacier numbers. Compared with best estimation, the simulated regional average ice volume has a small bias ranging from -  
 199 0.006 to 0.010  $km^3$ , especially for a zero bias when  $\beta = -0.4$ . This confirms the ability of OGGM to simulate the glaciers at

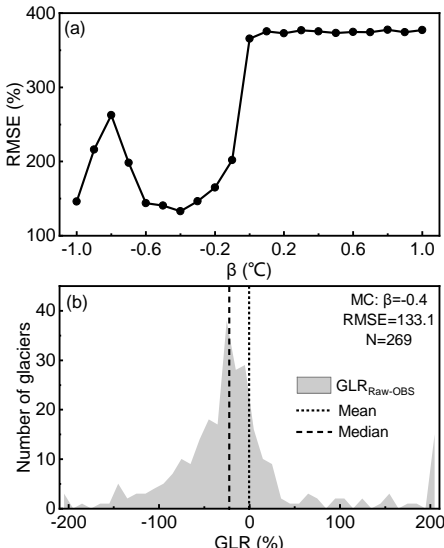
200 regional scale and  $\beta = -0.4$  is the best choice for our study.

201



202  
203 Figure 2. (a) The regional average glacier volume during the 5000-year spinup with various  $\beta$ . (b) The simulated regional  
204 average glacier volume from 900 to 2000 CE with different  $\beta$ . (c) The number of available glaciers with  
205 various  $\beta$ . (d) The simulated regional average  $GLR$  from 1100 to 1950 CE.

206



207  
208 Figure 3. (a) The RMSE of *maximum peak GLR* between the raw simulation results and mapped LIA glaciers for the MC  
209 experiment with various  $\beta$ . (b) The simulation bias distribution of *maximum peak GLR* for the MC experiment with  $\beta = -0.4$ .

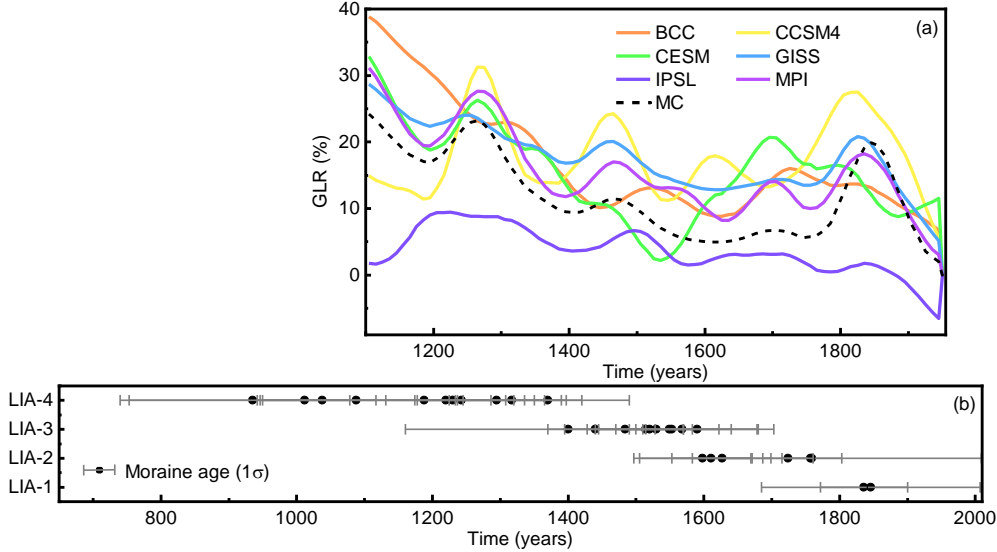
### 210 3.2 The pattern of glacier changes during the LIA

211 We would focus on the pattern of glacier changes during the LIA in MC experiment, but six GCM simulations are also  
212 shown in Fig. 4a for comparison. The simulation results in most experiments indicate four LIA glacial substages in BH, except  
213 for the CESM experiment losing LIA-3 substage. The timings of the four LIA glacial substages are 1270s (LIA-4), 1470s  
214 (LIA-3), 1710s (LIA-2), and 1850s (LIA-1) in MC experiment. These times vary slightly among the six GCM experiments,  
215 around 1230s - 1320s, 1470s - 1520s, 1620s - 1730s, 1800s - 1850s, respectively.

216 The most extensive glaciers occurred during LIA-4 in MC and six GCM experiments because our tuning strategy is to

217 ensure larger the regional average *GLR* at the early LIA. The *second peak GLR* occurred during LIA-1 in MC experiment. **This**  
 218 **founding is the same as** the results in the CCSM4, GISS, and MPI experiments but different from the results in BCC (LIA-2),  
 219 CESM (LIA-2), and IPSL (LIA-3) experiments. The *third and fourth peak GLR* occurred during LIA-3 and LIA-2 respectively  
 220 in MC experiment, also consistent with the simulations forced by CCSM4, GISS and MPI climate datasets.

221



222  
 223 Figure 4. (a) Time series of regional average *GLR* from 1100 to 1950 CE. (b) The observational timing when glaciers in the  
 224 monsoonal Himalaya reached their *maximum peak GLR*. We grouped the moraine ages based on their temporal distances to  
 225 each glacial substage simulated in MC experiment. The detailed information of the moraine ages measured by  $^{10}\text{Be}$  and  $^{14}\text{C}$   
 226 can be found in Table S1 and Xu & Yi (2014), respectively.

227 **4 Discussions**

228 **4.1 Comparison between Simulations and Observations**

229 We validated the simulation results using the moraine ages **across the monsoonal Himalaya** and mapped LIA glaciers  
 230 (Section 2.4). The simulated regional average *maximum peak GLR* (59.9%; Fig. 3b) in MC experiment agrees well with that  
 231 of mapped glaciers (60.6%). Similarly, the simulation results in BCC (57.8%), GISS (58.9%) and MPI (71.0%) experiments  
 232 are also consistent with observations. Observations from adjacent regions also support the simulation results (Qiao % Yi, 2017;  
 233 Zhang et al., 2018b). For example, Qiao & Yi (2017) found that the *maximum peak GLR* increased about 53.8 % during LIA  
 234 in the central and western Himalayas relative to 2015. Zhang et al. (2018b) reported a 71.5 % increase of *maximum peak*  
 235 *GLR* during LIA in the Gangdise Mountains relative to 2010, based on the glacial geomorphological maps. However, the  
 236 CCSM4 (99.0 %) and CESM (80.8 %) experiments overestimated the *maximum peak GLR* while the IPSL (32.1 %) experiment  
 237 underestimated it (Fig. S1). In addition, the negative bias for the median value in the simulations compared with observations  
 238 is identified in the MC and six GCM experiments (Fig. 3b and Fig. S1). The difference between the mean value and median  
 239 value indicates some **extrema** might impact the average.

240 Based on our tuning strategy (Murari et al., 2014; Xu & Yi et al., 2014), the *maximum peak GLR* occurred during LIA-4

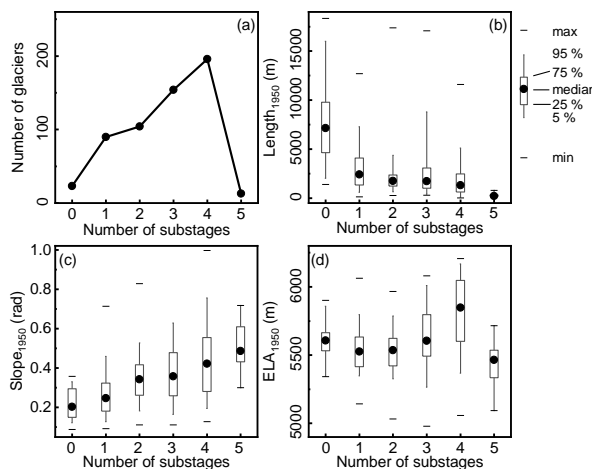
241 in MC experiment which is also confirmed by the dated moraine ages in monsoonal influenced Himalaya that the majority of  
242 glaciers advanced to their LIA maximum extents at the early LIA rather than the late LIA (Fig. 4b). Specifically, about 12 of  
243 the 30 moraine ages across the monsoonal Himalaya shows that the related glaciers reached their *maximum peak GLR* during  
244 LIA-4 compared with only 2 of them during LIA-1. However, there are still a large number of glaciers reaching their *maximum*  
245 *peak GLR* during LIA-3 (about 10 glaciers) and LIA-2 (about 6 glaciers). Ignoring the large uncertainties in the dating methods,  
246 the collective and individual differences in glacier changes are worth exploring. We will further discuss this issue in Section  
247 4.2.

248 The simulated number of LIA substages is also comparable with observations, including some moraine dating results and  
249 climatic proxy records. For example, Murari et al. (2014) and Zhang et al. (2018a) have identified four LIA moraines in  
250 Bhillangana and Dudhganga valleys, Garwal Himalaya, and Lopu Kangri Area, central Gangdise Mountains, respectively. Liu  
251 et al. (2017) have found at least three LIA moraines in Lhagoi Kangri Range, Karola Pass. Yang et al. (2003) found four cold  
252 phases during AD 1100-1150, 1500-1550, 1650-1700, and 1800-1850 over TP and eastern China according to the proxy data  
253 of paleoclimate. A regional moraine chronologies framework composed of  $^{14}\text{C}$ , lichenometry, and cosmogenic radionuclide  
254 ages found three substages during late-14<sup>th</sup>, 16<sup>th</sup> to early-18<sup>th</sup>, and late-18<sup>th</sup> to early-19<sup>th</sup>, corresponding to LIA-3, LIA-2, and  
255 LIA-1, respectively (Xu & Yi, 2014). However, the divergent number of LIA substages were also confirmed by some dating  
256 results and records. For example, only one moraine was dated in Cogarbu valley ( $1484 \pm 44$  CE; Table S1; Peng et al., 2019)  
257 and Shi Mo valley ( $1514 \pm 69$  CE; Table S1; Peng et al., 2020), but two substages were constrained in Lato valley, Lahul  
258 Himalaya (Saha et al., 2018), Langtang Khola valley, Nepal Himalaya (Barnard et al., 2006), and Gongotri Ganga valley,  
259 Garhwal Himalaya (Barnard et al., 2004). By applying dendroglaciology approach, Hochreuther et al. (2015) and Bräuning  
260 (2006) only detected one LIA substage in Gongpu glacier, Zepu glacier, Baitong glacier and Gyalaperi glacier, while more  
261 substages were found in Lhamcoka glacier (Bräuning, 2006), Xinpu glacier (Hochreuther et al., 2015), Gangapurna glacier,  
262 and Annapurna III glacier (Sigdel et al., 2020). Yi et al. (2008) identified three substages during AD 950-1820 based on 53  $^{14}\text{C}$   
263 dating ages.

#### 264 4.2 Why do four LIA substages exist in BH?

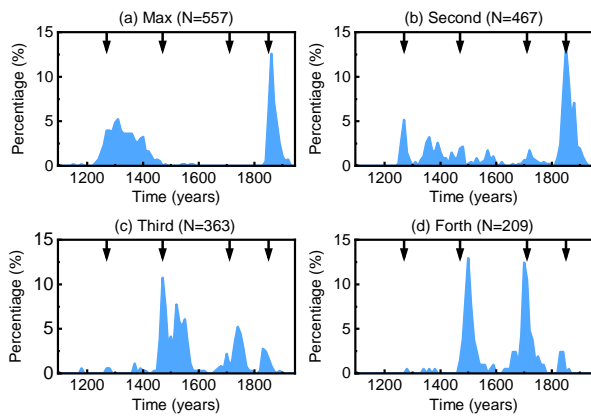
265 Clearly, MC experiment and GCM experiments (excluding CESM experiment) indicate four glacial substages over BH  
266 during LIA. However, due to the glacier individualities (different slopes and lengths), this does not mean each glacier in our  
267 study area exists four LIA substages (Fig. 5a), consistent with the moraine dating results. Instead, it just reflects that the  
268 majority of glaciers in BH have four glacial substages. For example, in MC experiment, only about 33.8 % glaciers have four  
269 substages during the LIA, while the rest glaciers are with zero (4.0 %), one (15.5 %), two (17.9 %), three (26.6 %) and five  
270 (2.2 %) substages. We argue that the difference in LIA substages is caused by the sensitivity of different glaciers despite many  
271 studies ascribed it to the different climate conditions (Owen & Dorch, 2014; Murari et al., 2014; Saha et al., 2019). Analysis

272 found the number of glacial substages are significantly correlated to the glacier properties (glacier length and slope). The  
 273 glacial substages numbers have significantly positive correlation with the glacier slopes while obviously negative correlation  
 274 with the glacier length (Fig. 5b, c). The correlation coefficient (CC) between the number of glacial substages and glacier length  
 275 at 1950 is -0.31 and the CC between the number of glacial substages and glacier slope at 1950 is 0.41. Both of the CCs can  
 276 pass 95% **significance** test. However, when zooming into the main glacial substages numbers (2, 3, 4), the relationship between  
 277 the number of glacial substages and glacier length does not become that clear (Fig. 5b). Therefore, we argue that glacial slope  
 278 may dominate the glacial substages numbers during LIA (Lüthi, 2009; Zekollari and Huybrechts, 2015; Bach et al., 2018; Eis  
 279 et al., 2019). The negative correlation between the glacier length and glacial substages numbers might be a result of the fact  
 280 that the longer (larger) glacier has a smaller slope (CC = -0.50). Besides, analysis also suggests weak relationship between  
 281 glacial substages numbers and glacial equilibrium-line altitude (ELA; Fig. 5d).  
 282



283  
 284 Figure 5. (a) The identified glacial substages number distribution in the MC experiment. The relationship between identified  
 285 glacial substages with (b) glacier length, (c) glacier slope, and (d) glacial ELA at 1950 in the MC experiment.  
 286

287 The occurrence time of each glacial substage also varies from glaciers, supported by the dispersal of moraine ages **across**  
 288 the monsoonal Himalaya (Fig. 4b). Notice that not all glaciers in BH reached their *maximum peak GLRs* during LIA-4, and  
 289 taking a step back, even among the glaciers with the *maximum peak GLR* during LIA-4, the occurrence times are also different  
 290 (Fig. 6a). Statistically, about 48.1 % glaciers experienced their *maximum peak GLR* during LIA-4 followed by 36.1 % glaciers  
 291 reaching their *maximum peak GLR* during LIA-1. Therefore, the occurrence time of *maximum peak GLR* at regional scale is  
 292 associated with the occurrence time of the majority of glaciers reaching their *maximum peak GLRs*. In addition, this can in  
 293 turn explain the lack of some moraines. Considering two glaciers both having four glacial substages but different occurrence  
 294 times of *maximum GLR peak* (one at LIA-4 and another at LIA-1) during LIA, we might find 4 moraines for the glacier which  
 295 reaches its *maximum GLR peak* at LIA-4 but only 1 moraine for the other because the first three moraines are destroyed by the  
 296 last glacier advance. Similarly, this phenomenon also remains in the occurrence times of the *second/third/fourth peak GLR*  
 297 (Fig. 6b-c).



300 Figure 6 The percentage of the glaciers with (a) *maximum peak GLR*, (b) the *second largest peak GLR*, (c) the *third largest peak GLR*, and (d) the *fourth largest peak GLR* over time in the MC experiment. The arrows represent the time of the four  
301 glacial substages, 1270s (LIA-4), 1470s (LIA-3), 1710s (LIA-2), and 1850s (LIA-1).

304 In summary, four LIA glacial substages at 1270s, 1470s, 1710s, and 1850s were found in BH based on the MC experiment.  
305 The maximum glacier extent appeared during LIA-4, **confirmed by** the moraine ages **in the monsoonal influenced Himalaya**.  
306 The regional glacial evolution is a collective effect of individual glacier changes. Four substages during LIA at the regional  
307 scale does not guarantee that each individual glacier has four substages. Likewise, not all glaciers in BH reached their *maximum*  
308 *peak GLRs* during LIA-4. Instead, it only represents the characteristics of most typical glaciers that accounted for the vast  
309 majority of the total glaciers. This can explain why there exists four substages in regional scale in the simulation but is hard  
310 captured in the previous studies that only focus on one individual glacier, which helps us to deeply understand the relationship  
311 between regional glacial evolution and the individual glacier response to climate change.

### 312 4.3 Climate-forcing Mechanisms

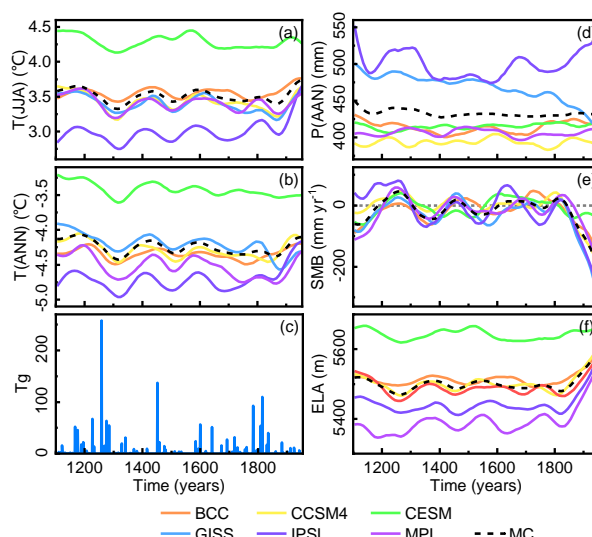
313 **The above discussions explained why there are four glacial substages in BH, but the climatic mechanisms behind these**  
314 **substages described here are still unclear.** A better understanding of the possible forcing mechanism of regional paleoglacier  
315 fluctuations at centennial timescales benefits projecting glacier outlooks in the future (Solomina et al., 2015). However, due  
316 to the limitation of field investigations, previous studies simply ascribed the glacier change to the temperature variation in the  
317 monsoon-influenced Himalaya by comparing the regional glacial sequences with the  $\delta^{18}\text{O}$  record from Greenland, Tibetan or  
318 North Atlantic (Peng et al., 2019, 2020). As the model can explicitly link the glacier changes with climate forcings (PDD  
319 scheme), it provides us an opportunity to further explore on this issue.

320 Our study revealed that the regional glacial fluctuations are related to the temperature changes rather than the precipitation  
321 change (Fig. 4a and Fig. 7a, b, d). Four cold intervals around 1320s, 1510s, 1760s, and 1870s in the MC experiment corresponds  
322 to LIA-4 (1270s), LIA-3 (1470s), LIA-2 (1710s), and LIA-1 (1850s), respectively. However, this signal cannot be detected in  
323 precipitation changes. Results from six GCM experiments also support this argument though with different time and strength.

324 The four cold intervals during the LIA in BH are forced by four large stratospheric sulfur-rich explosive eruptions events  
 325 (sulfate aerosol loadings  $> 60$  Tg; Fig. 7c; Gao et al., 2008) as the volcanic aerosols will inject abundant aerosol into the upper  
 326 atmosphere, cooling the climate (Schmidt et al., 2012). The beginning of oldest cold period (LIA-4) might be forced by a series  
 327 of volcanic activities, including a massive tropical volcanic eruption in 1257 followed by three smaller eruptions in 1268, 1275,  
 328 and 1284 (Miller et al., 2012). The volcanoes Billy Mitchell (1580), Huaynaputina (1600), Mount Parker (1641), Long Island  
 329 (1660), and Laki (1783) may contributed to the cooling events during LIA-3 and LIA-2 (Jonathan, 2007). The 1815 eruption  
 330 of Tambora and the 1883 eruption of Krakatau are believed to promote the youngest cold period of LIA (LIA-1; Rampino and  
 331 Self, 1982).

332 Although temperature determines whether BH can run into a glacial substage, precipitation still has the ability to regulate  
 333 the time of glacier advancing to its maximum in a glacial substage due to the fact that SMB is determined by the combination  
 334 of temperature and precipitation according to the PDD scheme (Eq. 1; Marzeion et al., 2012; Maussion et al., 2019). Positive  
 335 or negative SMB determines whether a glacier advances or retreats, and the amplitude of glacier change is directly influenced  
 336 by the amplitude of SMB change and the duration of the positive or negative SMB (Marzeion et al., 2012; Maussion et al.,  
 337 2019; Fig. 4a and Fig. 7e). Four peaks of SMB have been found in the MC experiment, around 1260s, 1460s, 1670s and 1820s,  
 338 corresponding to each substage. Stronger precipitation, associated with larger SMB, at the beginning of the cold interval will  
 339 drive the glacier advance rapidly, shortening the time for it to reach its maximum extent. In addition, we also found ELA has  
 340 a good correlation of the SMB, which can be used as a proxy for SMB. ELA is the elevation where accumulation equals  
 341 ablation for a certain glacier (Fig. 7f; Benn & Lehmkuhl, 2000; Heyman, 2014). Four periods of ELA dropping around 1270s  
 342 (-132.2 m), 1470s (-115 m), 1690s (-113.4 m), and 1820s (-112 m) are detected in the MC experiment, agreeing well with  
 343 SMB change. This finding, to some extent, would benefit field investigation as paleo ELA is easily available while paleo SMB  
 344 is hard to measure.

345



346

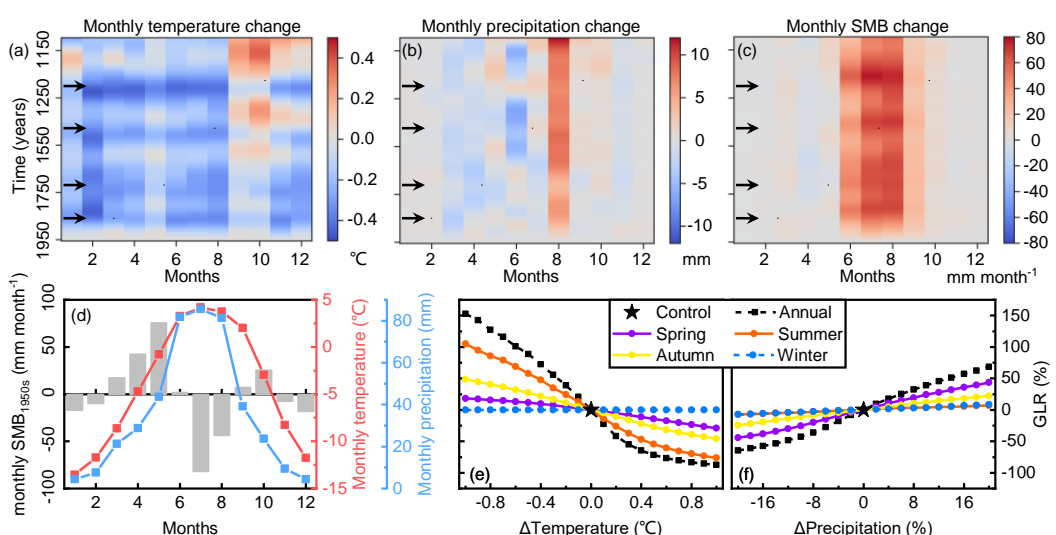
347 Figure 7. The regional average (a) summer temperature (T(JJA)), (b) annual temperature (T(ANN)), (d) annual precipitation  
 348 (P(ANN)), (e) SMB, (f) ELA from 1100 to 1950 CE at a decadal timescale. (c) Global stratospheric sulfate aerosol loadings  
 349 (Gao et al., 2008).

350

351 Seasonal climate is believed to have more important impacts on glacier evolutions than annual climate (Yan et al., 2020,  
 352 2021). We calculated the regional average monthly temperature, precipitation, cumulative SMB anomalies (relative to 1950s)  
 353 from 1100s to 1950s (Fig. 8a, b, and c) in the MC experiment to investigate the effect of monthly climate changes on glacial  
 354 fluctuation. Consistent with the Fig. 7e, four significant **increased** periods of monthly SMB changes around 1270s, 1470s,  
 355 1710s, and 1850s are identified (Fig. 8c) as a result of monthly temperature decreasing (Fig. 8a). Monthly precipitation does  
 356 not show obvious change, except for an abrupt increase in August (Fig. 8b). The abnormal increasing of August  
 357 precipitation is polluted by the GISS climate dataset which suffers from large precipitation bias.

358 Strong cumulative SMB change only occurs in JJA despite the temperature change almost uniformly distributes and  
 359 precipitation slightly variates (excluding August) throughout the year. The pattern of seasonal SMB change indicates that the  
 360 summer temperature might dominates the annual cumulative SMB. This is because JJA is the main ablation season of glaciers  
 361 in the monsoon-influenced Himalaya due to a higher temperature (Fig. 8d). A reduction of summer temperature will not only  
 362 decrease the number of positive degree days but also decrease the average temperature during the positive degree days,  
 363 resulting in the reduction in summer ablation (Eq. 1). Meanwhile, JJA is also the wettest season in the study area. Decreasing  
 364 temperature will lead to an increasing probability of solid precipitation, enhancing the accumulation. As the SMB is determined  
 365 by the sum of ablation and the accumulation, the JJA SMB is largely increased. However, though the temperature also decreases  
 366 in DJF, no more precipitation will not increase the accumulation. Therefore, the SMB change is weak.

367



368

369 Figure 8. The monthly (a) temperature, (b) precipitation, and (c) SMB changes relative to 1950s at a decadal timescale in the  
 370 MC experiment. The arrows in (a) – (c) represent the time of the four glacial substages, 1270s (LIA-4), 1470s (LIA-3), 1710s  
 371 (LIA-2), and 1850s (LIA-1). (d) the monthly temperature, precipitation, and SMB distribution in 1950s. Sensitivity of GLR to  
 372 annual or seasonal (e) temperature and (d) precipitation.

373

374 We also conducted a series of the sensitivity tests to examine the influence of seasonal temperature or precipitation on  
 375 BH glacier change (Fig. 8e, f). Glaciers retreats gradually as a response to the temperature increases or precipitation decreases.  
 376 The sensitivity of glaciers to temperature/precipitation changes – in the form of the rate of change for GLR per  $^{\circ}\text{C}/\%$   
 377 respectively – is highest for unmodified temperature/precipitation and decreases as they are varied further from the values  
 378 given in the historical climate runs. The average GLR changing rates are  $-160.1\text{ }^{\circ}\text{C}/\%$  and  $4.0\text{ }/\text{%/}\%$  for annual temperature and  
 379 precipitation changing respectively. The maximal sensitivity at unmodified temperature/precipitation is the expected case  
 380 due to the negative feedback mechanism of changing ELA as glacier length changes. Glaciers are most sensitive to summer  
 381 temperature change with an average change rate of  $110.4\text{ }^{\circ}\text{C}/\%$ , followed by autumn ( $51.6\text{ }^{\circ}\text{C}/\%$ ) and spring ( $25.2\text{ }^{\circ}\text{C}/\%$ ).  
 382 Glaciers are not sensitive to winter temperature change ( $0.0\text{ }^{\circ}\text{C}/\%$ ), supporting the results in Fig. 8c. This indicates that the  
 383 temperature changes in warm seasons, especially in summer, explain the most variance of the GLR changes. Fixing temperature,  
 384 the sensitivity of glaciers to precipitation changes is higher in spring ( $2.4\text{ }/\text{%/}\%$ ), followed by autumn ( $1.1\text{ }/\text{%/}\%$ ), summer  
 385 ( $0.4\text{ }/\text{%/}\%$ ) and winter ( $0.4\text{ }/\text{%/}\%$ ). Therefore, the precipitation change in spring and autumn has larger influences on glacier  
 386 evolution. In order to compare the relative sensitivity of temperature and precipitation to glacier change, we introduced an  
 387 index  $k = \frac{\Delta p}{\Delta T}$ , which is a measure of how much precipitation changes in response to temperature changes at present (Jeevanjee  
 388 and Romps, 2018). This is an index only related to the local climate and is about  $1.7\text{ }^{\circ}\text{C}/\%$  in the MC experiment. From our  
 389 sensitivity tests, we need a  $k = 53.0\text{ }^{\circ}\text{C}/\%$  to maintain the LIA glacier pattern (GLR =  $60.6\text{ }%$ ), which is much larger than  
 390 local climate  $k$ , indicating the temperature dominates the LIA glacial fluctuation in BH.

391 In summary, seasonal analysis and sensitivity tests indicate that the change in temperature, especially summer temperature,  
 392 is the dominant forcing factor for glacier changes during the LIA (sub-orbital scale) in monsoonal influenced Himalaya. In  
 393 contrast, the impact of precipitation change is limited. This conclusion has been drawn by Yan et al. (2020, 2021) at the orbital  
 394 scales, but now can be extends to the sub-orbital scale. In addition, we also found that the temperature changes during LIA are  
 395 closely related to volcanic activities (Gao et al., 2008; Miller et al., 2012; Schmidt et al., 2012).

## 396 5 Conclusions

397 We simulated the glacial evolution across BH during LIA using the coupled mass-balance and ice flow model, OGGM.  
 398 Compared with the geomorphological maps and moraine ages, OGGM broadly captures the pattern of glacier length change.  
 399 The regional pattern of glacier changes is the collective effect of each glacier. The dispersal of the observations could be  
 400 reproduced by the model due to the individualities of each glacier. On the regional scale, four LIA substages were identified  
 401 at about 1270s, 1470s, 1710s, and 1850s (from LIA-4 to LIA-1) in the MC experiment. The most extensive glacial advances  
 402 occurred during LIA-4, consistent with regional glacial chronological and geomorphic evidence. The number of glacial  
 403 substages for individual glacier has a positive correlation with glacier slope. The regional glacier advances are dominated by

404 the reduction of summer ablation.

405 Although limitations still exist in the simulations, such as the application of OGGM on **individual** glacier changes, this  
406 study presented the first simulation of sub-millennium glacial evolutions during LIA in BH using the OGGM. We found a  
407 testable relationship between seasonal climate change and glacier expansion, explained the dispersal of moraine ages and  
408 revealed the reasons for the four glacial substages during LIA in BH. Our findings link the limited observations with the model  
409 simulations and provide important insights into the climate forcing mechanism on glacier change at centennial timescale.

410 **Code and data availability.** Code to run OGGM v1.5.0 is available at <https://zenodo.org/record/4765924#.YnYuB4dBxD8>  
411 (Maussion et al., 2019).

412 **Author contributions.** Study concept devised by CW. YW performed the model runs and analysis, and wrote the original  
413 draft. LY and LG reviewed and revised the paper.

414 **Competing interests.** The authors declare that they have no conflicting interests.

415 **Acknowledgments.** This work was supported by the Second Tibetan Plateau Scientific Expedition and Research (STEP; grant  
416 no. 2019QZKK0205) and the National Natural Science Foundation (NSFC; grant no. 41771005, 41371082). We are grateful  
417 to Atle Nesje, Julia Eis, David Parkes, and one anonymous referee for their constructive comments/suggestions that help us a  
418 lot to improve the quality of the paper.

## 419 **References**

420 Bach, E., Radić, V., and Schoof, C.: How sensitive are mountain glaciers to climate change? Insights from a block model, *J  
421 Glaciol.*, 64(244), 247-258, <https://doi.org/10.1017/jog.2018.15>, 2018.

422 Balco, G., Stone, J.O., Lifton, N.A., and Dunai, T.J.: A complete and easily accessible means of calculating surface exposure  
423 ages or erosion rates from  $^{10}\text{Be}$  and  $^{26}\text{Al}$  measurements, *Quat. Geochronol.*, 3, 174-195,  
424 <https://doi.org/10.1016/j.quageo.2007.12.001>, 2008.

425 Barnard, P.L., Owen, L.A., Finkel, R.C., and Asahi, K.: Landscape response to deglaciation in a high relief, monsoon-  
426 influenced alpine environment, Langtang Himal, Nepal, *Quaternary. Sci. Rev.*, 25, 2162-2176,  
427 <https://doi.org/10.1016/j.quascirev.2006.02.002>, 2006.

428 Barnard, P.L., Owen, L.A., Sharma, M.C., and Finkel, R.C.: Late Quaternary (Holocene) landscape evolution of a monsoon-  
429 influenced high Himalayan valley, Gori Ganga, Nanda Devi, NE Garhwal, *Geomorphology*, 61, 91-110,  
430 <https://doi.org/10.1016/j.geomorph.2003.12.002>, 2004.

431 Benn, D.I., and Lehmkuhl, F.: Mass balance and equilibrium-line altitudes of glaciers in high-mountain environments, *Quatern.  
432 Int.*, 65/66, 15-29, [https://doi.org/10.1016/S1040-6182\(99\)00034-8](https://doi.org/10.1016/S1040-6182(99)00034-8), 2000.

433 Bräuning, A.: Tree-ring evidence of ‘Little Ice Age’ glacier advances in southern Tibet, *Holocene*, 16(3), 369-380,  
434 <https://doi.org/10.1191/0959683606hl922rp>, 2006.

435 Bueler, E., and Brown, J.: Shallow shelf approximation as a “sliding law” in a thermo mechanically coupled ice sheet model,

436 *J. Geophys. Res-Earth.*, 114, F03008, <https://doi.org/10.1029/2008JF001179>, 2009.

437 Carrivick, J.L., Boston, C.M., King, W., James, W.H., Quincey, D.J., Smith, M.W., Grimes, M., and Evans, J.: Accelerated  
438 volume loss in glacier ablation zones of NE Greenland, Little Ice Age to present, *Geophys. Res. Lett.*, 46, 1476–1484,  
439 <https://doi.org/10.1029/2018GL081383>, 2019.

440 Chandler, B.M.P., Boston, C.M., and Lukas, S.: A spatially-restricted Younger Dryas plateau icefield in the Gaick, Scotland:  
441 Reconstruction and palaeoclimatic implications, *Quaternary. Sci. Rev.*, 211, 107-135,  
442 <https://doi.org/10.1016/j.quascirev.2019.03.019>, 2019.

443 Chen, W., Yao, T., Zhang, G., Li, F., Zheng, G., Zhou, Y., and Xu, F.: Towards ice-thickness inversion: an evaluation of global  
444 digital elevation models (DEMs) in the glacierized Tibetan Plateau, *The Cryosphere*, 16, 197-281, <https://doi.org/10.5194/tc-16-197-2022>, 2022.

445 Dixit, A., Sahany, S., and Kulkarni, A.V.: Glacial changes over the Himalayan Beas basin under global warming, *J. Environ.  
446 Manage.*, 295, 113101, <https://doi.org/10.1016/j.jenvman.2021.113101>, 2021.

447 Dong, G., Zhou, W., Yi, C., Fu, Y., Zhang, L., and Li, M.: The timing and cause of glacial activity during the last glacial in  
448 central Tibet based on  $^{10}\text{Be}$  surface exposure dating east of Mount Jagang, the Xianza range, *Quaternary. Sci. Rev.*, 186, 284-  
449 297, <https://doi.org/10.1016/j.quascirev.2018.03.007>, 2018.

450 Dortch, J.M., Owen, L.A., and Caffee, M.W.: Timing and climatic drivers for glaciation across semi-arid western Himalayan-  
451 Tibetan orogen, *Quaternary. Sci. Rev.*, 78, 188-208, <http://dx.doi.org/10.1016/j.quascirev.2013.07.025>, 2013.

452 Eis, J., Maussion, F., and Marzeion, B.: Initialization of a global glacier model based on present-day glacier geometry and past  
453 climate information: an ensemble approach, *The Cryosphere*, 13, 3317-3335, <https://doi.org/10.5194/tc-13-3317-2019>, 2019.

454 Farinotti, D., Brinkerhoff, D. J., Clarke, G. K. C., Füst, J. J., Frey, H., Gantayat, P., Gillet-Chaulet, F., Girard, C., Huss, M.,  
455 Leclercq, P. W., Linsbauer, A., Machguth, H., Martin, C., Maussion, F., Morlighem, M., Mosbeux, C., Pandit, A., Portmann,  
456 A., Rabatel, A., Ramsankaran, R., Reerink, T. J., Sanchez, O., Stentoft, P. A., Singh Kumari, S., van Pelt, W. J. J., Anderson,  
457 B., Benham, T., Binder, D., Dowdeswell, J. A., Fischer, A., Helffricht, K., Kutuzov, S., Lavrentiev, I., McNabb, R.,  
458 Gudmundsson, G. H., Li, H., and Andreassen, L. M.: How accurate are estimates of glacier ice thickness? Results from ITMIX,  
459 the Ice Thickness Models Intercomparison eXperiment, *The Cryosphere*, 11, 949–970, <https://doi.org/10.5194/tc-11-949-2017>,  
460 2017.

461 **Farinotti, D., Huss, M., Fürst, J.J., Landmann, J., Machguth, H., Maussion, F., and Pandit, A.: A consensus estimate for the ice  
462 thickness distribution of all glaciers on Earth, *Nature Geoscience*, 12, 168-173, <https://doi.org/10.1038/s41561-019-0300-3>,  
463 2019.**

464 Fu, P., Stroeven, A.P., Harbor, J.M., Hättestrand, C., Heyman, J., Caffee, M.W., and Zhou, P.: Paleoglaciation of Shaluli Shan,  
465 southeastern Tibetan Plateau, *Quaternary. Sci. Rev.*, 64, 121-135, <http://dx.doi.org/10.1016/j.quascirev.2012.12.009>, 2013.

466 Furian, W., Maussion, F., and Schneider, C.: Projected 21st-Century Glacial Lake Evolution in High Mountain Asia, *Front.*

468 *Earth. Sci.*, 10, <https://doi.org/10.3389/feart.2022.821798>, 2022.

469 Chevalier, M-L., Hilley, G., Tapponnier, P., Woerd, J.V.D., Liu-Zeng, J., Finkel, R.C., Ryerson, F.J., Li, H., and Liu, X.:  
470 Constraints on the late Quaternary glaciations in Tibet from cosmogenic exposure ages of moraine ages. *Quaternary. Sci. Rev.*,  
471 30, 528-554, <https://doi.org/10.1016/j.quascirev.2010.11.005>, 2011.

472 Gao, C., Robock, A., Ammann, C.: Volcanic forcing of climate over the past 1500 years: An improved ice core-based index  
473 for climate models, *J. Geophys. Res.*, 113, D23111, <https://doi.org/10.1029/2008JD010239>, 2008.

474 Goosse, H., Barriat, P-Y., Dalaïden, Q., Klein, F., Marzeion, B., Maussion, F., Pelucchi, P., and Vlug, A.: Testing the  
475 consistency between changes in simulated climate and Alpine glacier length over the past millennium, *Clim. Past.*, 14, 1119-  
476 1133, <https://doi.org/10.5194/cp-14-1119-2018>, 2018.

477 Greve, R.: A continuum-mechanical formulation for shallow polythermal ice sheets. *Philos. T.R. Soc. A.*, 355(1726), 921-974,  
478 [https://doi.org/10.1175/1520-0442\(1997\)010<0901:AOAPTD>2.0.CO;2](https://doi.org/10.1175/1520-0442(1997)010<0901:AOAPTD>2.0.CO;2), 1997a.

479 Greve, R.: Application of a polythermal three-dimensional ice sheet model to the Greenland ice sheet: Response to steady-  
480 state and transient climate scenarios, *J. Climate.*, 10(5), 901-918, <https://doi.org/10.1098/rsta.1997.0050>, 1997b.

481 Grove, J.M.: *Little Ice Age*, 2 ed, Routledge, 2013.

482 Harris, I., Osborn, T.J., Jones, P., and Lister, D.: Version 4 of the CRU TS monthly high-resolution gridded multivariate climate  
483 dataset, *Sci. Data*, 7, 109, <https://doi.org/10.1038/s41597-020-0453-3>, 2020.

484 Heyman, J.: Paleoglaciation of the Tibetan Plateau and surrounding mountains based on exposure ages and ELA depression  
485 estimates, *Quaternary. Sci. Rev.*, 91, 30-41, <http://dx.doi.org/10.1016/j.quascirev.2014.03.018>, 2014.

486 Heyman, J., Stroeven, A.P., Harbor, J.M., and Caffee, M.W.: Too young or too old: Evaluating cosmogenic exposure dating  
487 based on an analysis of compiled boulder exposure ages, *Earth. Planet. Sc. Lett.*, 302, 71-80,  
488 <https://doi.org/10.1016/j.epsl.2010.11.040>, 2011.

489 Hochreuther, P., Loibl, D., Wernicke, J., Zhu, H., Grießinger, J., and Bräuning, A.: Ages of major Little Ice Age glacier  
490 fluctuations on the southeast Tibetan Plateau derived from tree-ring-based moraine dating, *Palaeogeogr. Palaeocl.*, 422, 1-10,  
491 <http://dx.doi.org/10.1016/j.palaeo.2015.01.002>, 2015.

492 Jarvis, A., Reuter, H., Nelson, A., and Guevara, E.: Hole-filledSRTM for the globe Version 4, CGIAR Consortium for Spatial  
493 Information, University of Twente, 2008.

494 Jeevanjee, N., and Romps, D.M.: Mean precipitation change from a deepening troposphere, *P Natl. Acad. Sci. USA*, 115(45),  
495 11465-11470, <https://doi.org/10.1073/pnas.1720683115>, 2018.

496 Jonathan, C.: Climate change: biological and human aspects. Cambridge University Press. P. 164. ISBN 978-0-521-69619-7,  
497 2007.

498 Lifton, N., Sato, T., and Dunai, T.J.: Scaling in situ cosmogenic nuclide production rates using analytical approximations to  
499 atmospheric cosmic-ray fluxes, *Earth. Planet. Sc. Lett.*, 386, 149-160, <http://dx.doi.org/10.1016/j.epsl.2013.10.052>, 2014.

500 Lipscomb, W.H., Price, S.F., Hoffman, M.J., Leguy, G.R., Bennett, A.R., Bradley, S.L., Evans, K.J., Fyke, J.G., Kennedy, J.H.,  
501 Perego, M., Ranken, D.M., Sacks, W.J., Salinger, A.G., Vargo, L.J., and Worley, P.J.: Description and evaluating of the  
502 Community Ice Sheet Model (CISM) v2.1, *Geosci. Model. Dev.*, 12, 387-424, <https://doi.org/10.5194/gmd-12-387-2019>, 2019.  
503 Liu, J., Yi, C., Li, Y., Bi, W., Zhang, Q., and Hu, G.: Glacial fluctuations around the Karola Pass, eastern Lhagai Kangri Range,  
504 since the Last Glacial Maximum, *J. Quaternary. Sci.*, 32(4), 516-527, <https://doi.org/10.1002/jqs.2946>, 2017.  
505 Lüthi, M.P.: Transient response of idealized glaciers to climate variations, *J. Glaciol.*, 55(193), 918-903,  
506 <https://doi.org/10.3189/002214309790152519>, 2009.  
507 Marzeion, B., Jarosch, A. H., and Hofer, M.: Past and future sea-level change from the surface mass balance of glaciers, *The  
508 Cryosphere*, 6, 1295–1322, <https://doi.org/10.5194/tc-6-1295-2012>, 2012.  
509 Maussion, F., Butenko, A., Champollion, N., Dusch, M., Eis, J., Fourteau, K., Gregor, P., Jarosch, A. H., Landmann, J., Oesterle,  
510 F., Recinos, B., Rothenpieler, T., Vlug, A., Wild, C. T., and Marzeion, B.: The Open Global Glacier Model (OGGM) v1.1,  
511 *Geosci. Model Dev.*, 12, 909–931, <https://doi.org/10.5194/gmd-12-909-2019>, 2019.  
512 Miller, G.H., Geirsdóttir, Á., Zhong, Y., Larsen, D.J., Otto-Bliesner, B.L., Holland, M.M., Bailey, D.A., Refsnider, K.A.,  
513 Lehman, S.J., Southon, J.R., Anderson, C., Björnsson, H., and Thordarson, T.: Abrupt onse of the Little Ice Age triggered by  
514 volcanism and sustained by sea-ice/ocean feedbacks, *Geophys. Res. Lett.*, 39, L02708, <https://doi.org/10.1029/2011GL050168>,  
515 2012.  
516 Murari, M.K., Owen, L.A., Dortch, J.M., Caffee, M.W., Dietsch, C., Fuchs, M., Haneberg, W.C., Sharma, M.C., and Townsend-  
517 Small, A.: Timing and climatic drivers for glaciation across monsoon-influenced regions of the HimalayaneTibetan orogen,  
518 *Quaternary. Sci. Rev.*, 88, 159-182, <http://dx.doi.org/10.1016/j.quascirev.2014.01.013>, 2014.  
519 Oerlemans, J., Anderson, B., Hubbard, A., Huybrechts, Ph., Jóhannesson, T., Knap, W.H., Schmeits, M., Stroeven, A.P., van  
520 de Wal, R.S.W., and Zuo, Z.: Modelling the response of glaciers to climate warming, *Climate Dynamics*, 14, 267-274,  
521 <https://doi.org/10.1007/s003820050222>, 1998.  
522 Owen, L.A.: Latest Pleistocene and Holocene glacier fluctuations in the Himalaya and Tibet, *Quaternary. Sci. Rev.*, 28, 2150-  
523 2164, <https://doi.org/10.1016/j.quascirev.2008.10.020>, 2009.  
524 Owen, L.A., and Dortch, J.M.: Nature and timing of Quaternary glaciation in the Himalayan-Tibetan orogen, *Quaternary. Sci.  
525 Rev.*, 88, 14-54, <http://dx.doi.org/10.1016/j.quascirev.2013.11.016>, 2014.  
526 PAGES 2k-PMIP3 group.: Continental-scale temperature variability in PMIP3 simulations and PAGES 2k regional  
527 temperature reconstructions over the past millennium, *Clim. Past.*, 11, 1673-1699, <https://doi.org/10.5194/cp-11-1673-2015>,  
528 2015.  
529 Parkes, D., and Goosse, H.: Modelling regional glacier length changes over the last millennium using the Open Global Glacier  
530 Model, *The Cryosphere*, 14, 3135-3153, <https://doi.org/10.5194/tc-14-3135-2020>, 2020.  
531 Pelto, B.M., Maussion, F., Menounos, B., Radić, V and Zeuner, M.: Bias-corrected estimates of glacier thickness in the

532 Columbia River Basin, Canada, *J. Glaciol.*, 66(260), 1051-1063, <https://doi.org/10.1017/jog.2020.75>, 2020.

533 Peng, X., Chen Y., Liu, G., Liu, B., Li, Y., Liu, Q., Han, Y., Yang, W., and Cui, Z.: Late Quaternary glaciations in the Cogarbu  
534 valley, Bhutanese Himalaya, *J. Quaternary. Sci.*, 34(1), 40-50, <http://dx.doi.org/10.1002/jqs.3079>, 2019.

535 Peng, X., Chen, Y., Li, Y., Liu, B., Liu, Q., Yang, W., Liu, G.: Late Holocene glacier fluctuations in the Bhutanese Himalaya,  
536 *Global. Planet. Change.*, 187, 103137, <https://doi.org/10.1016/j.gloplacha.2020.103137>, 2020.

537 Pronk, J.B., Bolch, T., King, W., Wouters, B., and Benn, D.I.: Contrasting surface velocities between lake- and land-terminating  
538 glaciers in the Himalayan region, *The Cryosphere*, 15, 5577-5599, <https://doi.org/10.5194/tc-15-5577-2021>, 2021.

539 Qiao, B., and Yi, C.: Reconstruction of Little Ice Age glacier area and equilibrium line attitudes in the central and western  
540 Himalaya, *Quatern. Int.*, 444, 65-75, <http://dx.doi.org/10.1016/j.quaint.2016.11.049>, 2017.

541 Qureshi, M.A., Li, Y., Yi, C., and Xu, X.: Glacial changes in the Hunza Basin, western Karakoram, since the Little Ice Age,  
542 *Palaeogeogr. Palaeocl.*, 562, 110086, <https://doi.org/10.1016/j.palaeo.2020.110086>, 2021.

543 Rampino, M.R., and Self, S.: Historic Eruptions of Tambora (1815), Krakatau (1883), and Agung (1963), their Stratospheric  
544 Aerosols, and Climatic Impact, *Quatern. Res.*, 18, 127-143, [https://doi.org/10.1016/0033-5894\(82\)90065-5](https://doi.org/10.1016/0033-5894(82)90065-5), 1982.

545 RGI Consortium.: Randolph Glacier Inventory (RGI)-A Dataset of Global Glacier Outlines: Version 6.0,  
546 <https://doi.org/10.7265/N5-RGI-60>, 2017.

547 Saha, S., Owen, L.A., Orr, E.N., and Caffee, M.W.: High-frequency Holocene glacier fluctuations in the Himalayan-Tibetan  
548 orogen, *Quaternary. Sci. Rev.*, 220, 372-400, <https://doi.org/10.1016/j.quascirev.2019.07.021>, 2019.

549 Saha, S., Owen, L.A., Orr, E.N., & Caffee, M.W.: Timing and nature of Holocene glacier advances at the northwestern end of  
550 the Himalayan-Tibetan orogen, *Quaternary. Sci. Rev.*, 187, 177-202, <https://doi.org/10.1016/j.quascirev.2018.03.009>, 2018.

551 Schmidt, G. A., Jungclaus, J. H., Ammann, C. M., Bard, E., Braconnot, P., Crowley, T. J., Delaygue, G., Joos, F., Krivova,  
552 N.A., Muscheler, R., Otto-Bliesner, B.L., Pongratz, J., Shindell, D.T., Solanki, S.K., Steinhilber, F., and Vieira, L.E.A.: Climate  
553 forcing reconstructions for use in PMIP simulations of the last millennium (v1.0), *Geosci. Model. Dev.*, 4, 33-45,  
554 <https://doi.org/10.5194/gmd-4-33-2011>, 2012.

555 Shafeeqe, M., and Luo, Y.: A multi-perspective approach for selecting CMIP6 scenarios to project climate change impacts on  
556 glacio-hydrology with a case study in Upper Indus River basin, *J. Hydrol.*, 599, 126466,  
557 <https://doi.org/10.1016/j.jhydrol.2021.126466>, 2021.

558 Sigdel, S.R., Zhang, H., Zhu, H., Muhammad, S., and Liang, E.: Retreating glacier and advancing forest over the past 200  
559 years in the Central Himalayas, *J. Biogeogr.*, 125, e2020JG005751. <https://doi.org/10.1029/2020JG005751>, 2020.

560 Solomina, O.N., Bradley, R.S., Hodgson, D.A., Ivy-Ochs, S., Jomelli, V., Mackintosh, A.N., Nesje, A., Owen, L.A., Wanner,  
561 H., Wiles, G.C., and Young, N.E.: Holocene glacier fluctuations, *Quaternary. Sci. Rev.*, 111, 9-34,  
562 <http://dx.doi.org/10.1016/j.quascirev.2014.11.018>, 2015.

563 Taylor, K., Stouffer, R., and Meehl, G.: An Overview of CMIP5 and the Experiment Design, *B. Am. Meteorol. Soc.*, 93, 485-

564 498, <https://doi.org/10.1175/BAMS-D-11-00094.1>, 2012.

565 **WGMS: Fluctuations of Glaciers Database**.World Glacier Monitoring Service, Zurich, Switzerland,  
566 <https://doi.org/10.5904/wgmsfog-2017-10>, 2017.

567 Winkelmann, R., Martin, M.A., Haseloff, M., Albrecht, T., Bueler, E., Khroulev, C., and Levermann, A.: The Potsdam Parallel  
568 Ice Sheet Model (PISM-PIK) – Part 1: Model description, *The Cryosphere*, 5, 715-726, <https://doi.org/10.5194/tc-5-715-2011>,  
569 2011.

570 Xu, X., and Yi, C.: Little Ice Age on the Tibetan Plateau and its bordering mountains: Evidence from moraine chronologies,  
571 *Global. Planet. Change.*, 116, 41-53, <http://dx.doi.org/10.1016/j.gloplacha.2014.02.003>, 2014.

572 Yan, Q., Owen, L. A., Wang, H., and Zhang, Z.: Climate constraints on glaciation over High-Mountain Asia during the last  
573 glacial maximum, *Geophys. Res. Lett.*, 45, 9024–9033, <https://doi.org/10.1029/2018GL079168>, 2018.

574 Yan, Q., Owen, L. A., Zhang, Z., Wang, H., Wei, T., Jiang, N., and Zhang, R.: Divergent evolution of glaciation across High-  
575 Mountain Asia during the last four glacial-interglacial cycles, *Geophys. Res. Lett.*, 48, e2021GL092411,  
576 <https://doi.org/10.1029/2021GL092411>, 2021.

577 Yan, Q., Owen, L.A., Zhang, Z., Jiang, N., and Zhang, R.: Deciphering the evolution and forcing mechanisms of glaciation  
578 over the Himalayan-Tibetan orogen during the past 20,000 years, *Earth. Planet. Sc. Lett.*, 541, 116295,  
579 <https://doi.org/10.1016/j.epsl.2020.116295>, 2020.

580 Yang, B., Achim, B., and Shi, Y.: Late Holocene temperature fluctuations on the Tibetan Plateau, *Quaternary. Sci. Rev.*, 22,  
581 2335-2344, [https://doi.org/10.1016/S0277-3791\(03\)00132-X](https://doi.org/10.1016/S0277-3791(03)00132-X), 2003.

582 Yi, C., Chen, H., Yang, J., Liu, B., Fu, P., Liu, K., and Li, S.: Review of Holocene glacial chronologies based on radiocarbon  
583 dating in Tibet and its surrounding mountains, *J. Quaternary. Sci.*, 23(6-7), 533-543, <https://doi.org/10.1002/jqs.1228>, 2008.

584 Zekollari, H., and Huybrechts, P.: On the climate–geometry imbalance, response time and volume–area scaling of an alpine  
585 glacier: insights from a 3-D flow model applied to Vadret da Morteratsch, Switzerland, *Ann. Glaciol.*, 56(70), 51-62,  
586 <https://doi.org/10.3189/2015AoG70A921>, 2015.

587 Zhang, Q., Yi, C., Dong, G., Fu, P., Wang, N., and Capolongo, D.: Quaternary glaciations in the Lopu Kangri area, central  
588 Gangdise Mountains, southern Tibetan Plateau, *Quaternary. Sci. Rev.*, 201, 470-482,  
589 <https://doi.org/10.1016/j.quascirev.2018.10.027>, 2018a.

590 Zhang, Q., Yi, C., Fu, P., Wu, Y., Liu, J., and Wang, N.: Glacier change in the Gangdise Mountains, southern Tibet, since the  
591 Little Ice Age, *Geomorphology*, 306, 51-63, <https://doi.org/10.1016/j.geomorph.2018.01.002>, 2018b.